Journal of Biomedical Optics

BiomedicalOptics.SPIEDigitalLibrary.org

Hyperspectral imaging for detection of arthritis: feasibility and prospects

Matija Milanic
Lukasz A. Paluchowski
Lise L. Randeberg

SPIE.

Journal of Biomedical Optics 20(9), 096011 (September 2015)

Hyperspectral imaging for detection of arthritis: feasibility and prospects

Matija Milanic, Lukasz A. Paluchowski, and Lise L. Randeberg*
Norwegian University of Science and Technology, Department of Electronics and Telecommunications, 7491 Trondheim, Norway

Abstract. Rheumatoid arthritis (RA) is a disease that frequently leads to joint destruction. It has a high incidence rate worldwide, and the disease significantly reduces patients' quality of life. Detecting and treating inflammatory arthritis before structural damage to the joint has occurred is known to be essential for preventing patient disability and pain. Existing diagnostic technologies are expensive, time consuming, and require trained personnel to collect and interpret data. Optical techniques might be a fast, noninvasive alternative. Hyperspectral imaging (HSI) is a noncontact optical technique which provides both spectral and spatial information in one measurement. In this study, the feasibility of HSI in arthritis diagnostics was explored by numerical simulations and optimal imaging parameters were identified. Hyperspectral reflectance and transmission images of RA and normal human joint models were simulated using the Monte Carlo method. The spectral range was 600 to 1100 nm. Characteristic spatial patterns for RA joints and two spectral windows with transmission were identified. The study demonstrated that transmittance images of human joints could be used as one parameter for discrimination between arthritic and unaffected joints. The presented work shows that HSI is a promising imaging modality for the diagnostics and follow-up monitoring of arthritis in small joints. [DOI: 10.1117/1.JBO.20.9.096011]

Keywords: Monte Carlo; hyperspectral imaging; arthritis; light–tissue interaction; diffuse reflectance spectroscopy.

Paper 150255PR received Apr. 14, 2015; accepted for publication Aug. 17, 2015; published online Sep. 11, 2015.

1 Introduction

Rheumatoid arthritis (RA) is a destructive inflammatory polyarthritis with a prevalence of 1% to 2%. It leads to joint destruction and deformation, which results in loss of function. Because hand and finger joints are often affected, the progress of the disease severely affects the patient's quality of life. Untreated or insufficiently treated arthritis often leads to disability including an inability to work.

The functional outcome and subsequently the indirect costs are strongly dependent on the time lag between the onset of the disease and the beginning of the treatment. For example, in 2004, the indirect costs were estimated at 1260 to 37,994 EUR annually (variations are due to different countries and healthcare systems), accounting for a half to three quarters of the total cost.[1] Several studies have shown that a window of opportunity exists in the first year and especially in the first 3 months, in which a treatment has a higher likelihood for improving the course of the disease.[2] Specifically, after 3 months of symptoms, the immunopathological processes in the RA synovium become typical for RA and very similar in patients with longer disease durations.[3] Therapy after this period with disease-modifying antirheumatic drugs and also with biological drugs targeting TNF-α reduces disease activity and limits the development of damage, but it does not cure RA. Recent studies show that the very early phase of RA synovitis represents a pathologically different stage of disease, and that very early intervention using the same drugs may qualitatively have a different effect compared with later intervention.[4] Therefore, early diagnosis and therapeutic intervention should focus on the detection and stopping of the disease in order to prevent irreversible damage. However, to be able to do early diagnostics, it is important to know the characteristic markers for established arthritis as a starting point for developing sensitive and specific diagnostic algorithms.

Currently, x-ray, ultrasound, scintigraphy, and magnetic resonance are used as imaging modalities for diagnosis of arthritis.[5] All these techniques have drawbacks such as the need for ionizing radiation and low sensitivity in early arthritis for x-ray; high variability between operators and long examination time for thorough imaging of multiple joints for ultrasound; high costs, long intermediate examination time, and limited availability for magnetic resonance imaging (MRI). An imaging modality for diagnosis of arthritis addressing all these drawbacks is thus needed.

Reports about using optical techniques for imaging of arthritic joints can be found in the literature.[5–8] However, the reported techniques utilized monochromatic light, and thus did not explore the richness of the spectral information obtained using a broadband light. Spectroscopic data carry useful information about tissue optical properties such as absorption, scattering, and tissue composition. Specifically for an arthritic joint, the features, which can significantly alter spectral information, include vessel proliferation (increased hemoglobin concentration), hypoxia, and quantitative and qualitative change of synovial fluid (SF) (edema, increased scattering). In addition, a joint shape changes when the synovial membrane thickens and SF collections are present. More specific details about the changes typical for an arthritic joint can be found in the Background and

*Address all correspondence to: Lise L. Randeber, E-mail: lise.randeberg@iet.ntnu.no

Methods sections. Thus, by considering both spectral and spatial data, the reliability of the arthritis diagnosis could be increased. A suitable spectral imaging modality for arthritis diagnostics is hyperspectral imaging (HSI). The technique provides both spectral and spatial information in one measurement and does not require contact between the object and the sensor. It has been demonstrated that the technique is very sensitive for detecting pathological conditions such as hypoxia[9] or enhanced vascularization,[10] both being important characteristics of an arthritic joint. In addition, the technique is not harmful to the patient (no ionizing radiation), is fast, and does not depend on the operator's experience. The cost is less than MRI or x-ray and is probably comparable to ultrasound.

The main objective of this study was to explore the feasibility of HSI in arthritis diagnostics and to identify optimal imaging parameters for further experimental studies. Hyperspectral reflectance and transmission images of joints were simulated for multiple wavelengths in the spectral range between 600 and 1100 nm with wavelength steps of 10 nm. This spectral range was selected due to the optical properties of apparent tissue chromophores (hemoglobin, water, and melanin). The chosen wavelength range is within the so-called optical window for tissue imaging as the optical penetration depth is at its maximum in this spectral range. The present study is a part of the Iacobus project (EC 7th Framework Programme, Grant No. 305760). The aim of this project is to develop an imaging modality based on HSI and photoacoustic imaging for early diagnosis of arthritis in human finger joints.

2 Background

The cause of rheumatoid arthritis is unknown. Immunological and inflammatory processes leading to subsequent tissue destruction are set off at the very beginning of the disease. Symptoms include swelling, stiffness, pain, and subsequent thickening of the synovial membrane and joint destruction (Fig. 1). To be able to simulate photon transport in an affected joint, it is a prerequisite to be able to quantify these effects. A literature study was carried out to unveil the data needed for this study. Only a brief summary is included here, and further information can be found in the given references.

Volume quantification of the synovial membrane in metacarpophalangeal (MCP) joints in patients with RA and healthy controls has been performed by contrast-enhanced MRI.[11] In each of the four MCP joints, the median synovial membrane was found to be on average 30 times larger in the clinically active joints (0.54 to 0.97 ml) as compared to the healthy controls (0.01 to 0.07 ml).

Fig. 1 A photograph showing an acute arthritis phase in the proximal interphalangeal joint of the middle finger.

The capillary distribution in the affected joints will change.[12] The reported blood volume fraction was 2.9% in the normal synovia and 1.2% in the RA synovia. However, the total number of vessels in arthritic joints is increased due to thickening of the synovia.

Hypoxia is a significant feature of RA in addition to inflammation. The median oxygen partial pressure in RA synovium was found to be 26 mmHg (saturation 48%),[13] as compared to 74 mmHg (saturation 95%) in normal synovium.[14]

The volume of SF in human finger joints is small and there are no reliable quantitative reports on it. However, it was found from inspection of MRI images that the volume of the SF in finger joints significantly increases when inflammation is presented in a joint.[11] The appearance of the synovial liquid turns from clear in healthy joints, to turbid and yellow or pink in early arthritic inflammation.[15,16] This indicates a significant change in the optical properties of the SF.

Another characteristic of RA is destruction of cartilage. The average thickness of cartilage in a healthy finger joint has been measured to be 0.40 ± 0.12 mm with a maximum of 0.67 ± 0.14 mm.[17] The water content has also been found to change in cartilage affected by arthritis. It was reported that there is an increase in water content from the average normal of 60% to 85% to greater than 90%.[18]

3 Methods

3.1 *Joint Geometry and Optical Properties*

The above information about human joint physiology and anatomy was used to construct human joint models. The models consisted of geometry including dimensions, tissue distributions, and corresponding optical properties.

Four joint models were constructed; specifically, one healthy and three arthritic finger joints. The geometry of a healthy finger joint (Fig. 2) was constructed using data from computed tomography and MRI images[19] to anatomically provide correct dimensions and tissue distributions. The healthy finger model simulated in this study represents one possible normal finger anatomy as the thicknesses, length, and other features might substantially vary.[20] However, the constructed model serves as a representative of a healthy, normal finger and it should be sufficient to explore the general properties of healthy human fingers. The volume of interest (VOI) represented a proximal interphalangeal joint from approximately half of the proximal phalanx and to approximately half of the intermediate phalanx. The size of the VOI was $20 \times 40 \times 20$ mm^3 (coordinates x, y, and z), with a spatial discretization of 0.1 mm. The geometry involved 10 different tissue types, all of them marked in Fig. 2.

The affected joints were modeled by varying the base geometry of the normal joint according to the expected physiological/morphological changes in an arthritic joint presented in the Background section. The purpose of varying the base geometry was to study how specific pathological processes ongoing in RA joints affect the optical properties, and thus the spectra. Three different variants of arthritic joints were simulated: an arthritic joint with SF effusion (SF model), an arthritic joint with synovial membrane thickening (SM model), and an arthritic joint with both SF effusion and synovial membrane thickening

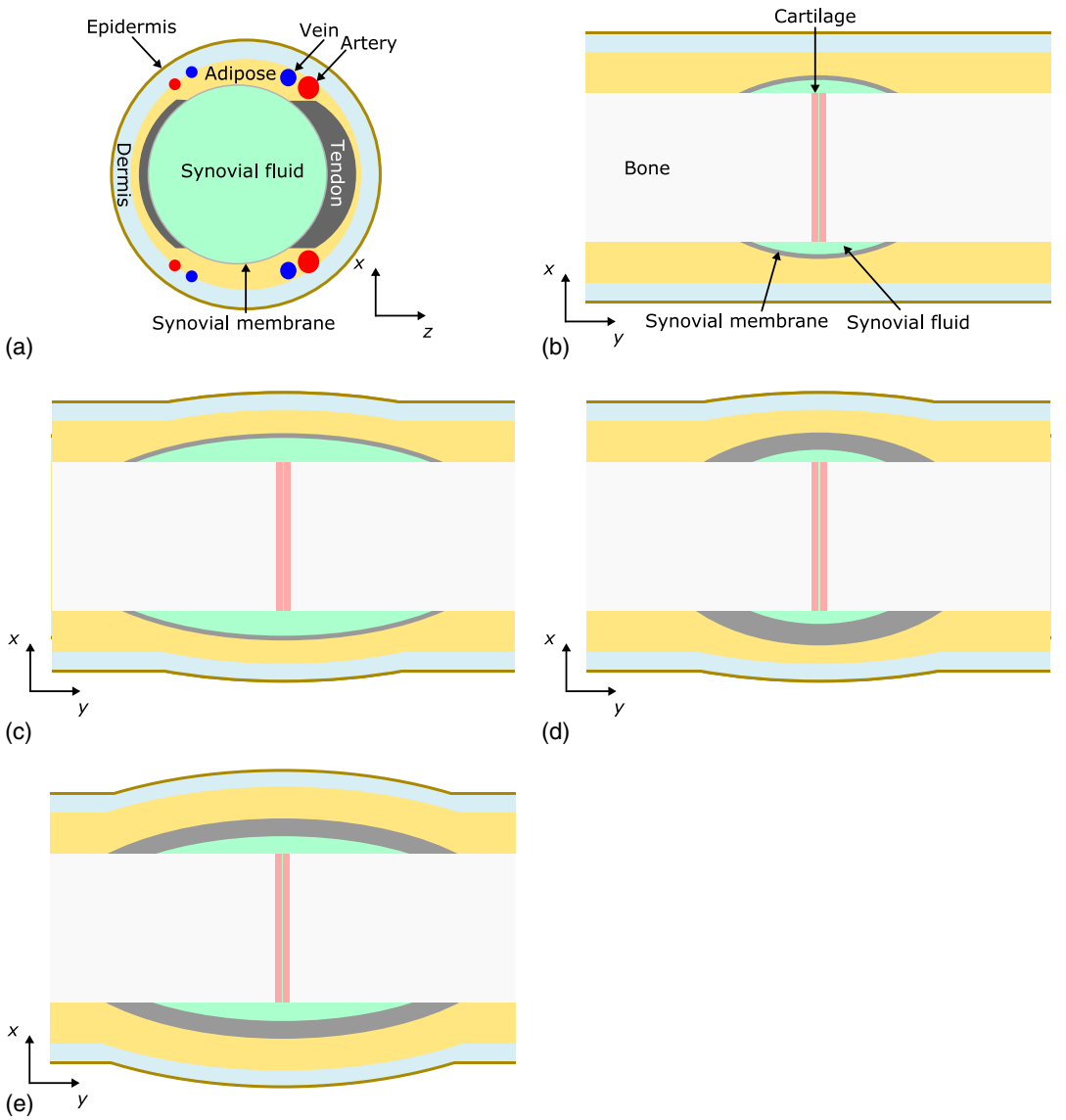

Fig. 2 (a) Cross section *xz*-plane through the geometry at the middle of the joint. (b) Cross section xy-plane at the middle of the geometry for the healthy joint, (c) synovial fluid effusion – SF, (d) synovial membrane thickening – SM, and (e) synovial fluid effusion and synovial membrane thickening – SFM models. The joint tissue is marked with the corresponding labels. The healthy joint model was constructed using data from computed tomography and magnetic resonance imaging (MRI) images available in Ref. 19.

(SFM model). The modifications of the base geometry are presented in Table 1 and Figs. 2(c) to 2(e).

For all simulated tissues, the corresponding optical properties (μ_a, μ_s, g, and n) were found in the literature, except for the SF. The properties of the latter were measured in our laboratory,[21] as there were no reliable reports available. Brief information about the optical properties used in the simulation including comments and references is presented in Table 2. The absorption coefficients of a specific tissue was calculated as a linear combination of absorption coefficients of chromophores present in that tissue weighted with the corresponding volume concentrations. The absorption and reduced scattering coefficients of the simulated chromophores are presented in Fig. 3. The simulated tissue properties for the different models are listed in corresponding columns, N, SF, SM, and SFM. A detailed explanation of the optical properties can be found in Milanic et al.[21]

3.2 *Optical Transport Model*

To simulate photon transport in small volumes of skin, a custom weighted-photon, three-dimensional Monte Carlo (MC) model was used.[23] In the weighted-photon MC model, a large number of photon packets propagate through the tissue and deposit a fraction of their energy into specific volume elements, according to the local absorption properties, or escape from the simulated volume according to the local refraction index. Stochastic relations are used to determine each photon's random path, according to the physical laws of light scattering, reflection, and refraction. Specifics of these relations depend on the optical properties of the involved tissues. With an increasing number of simulated photons and ever finer spatial discretization of the treated volume, the results of the simulation ideally converge toward the correct values. Implementing the weighted-photon

Table 1 Modification of the normal joint geometry to simulate affected joint models and corresponding volume of interest (VOI).

Model	Volume change factor	VOI (mm^3)
SF	Synovial fluid 7.5×	$24.4 \times 40.0 \times 24.4$
SM	Synovial membrane 30×	$24.2 \times 40.0 \times 24.2$
SFM	Synovial fluid 7.5×	$26.8 \times 40.0 \times 26.8$
	Synovial membrane 30×	

MC model in three dimensions allows simulation of light transport within tissues or organs of arbitrary complex shape and optical heterogeneity.

The mirror boundary condition (BC) was used at the xz plane boundaries of the VOI. Thus, the photons reflected from the side boundaries improved the statistics of the simulation. The mirror BC is an appropriate approach for this study, because an infinitely wide beam irradiation was simulated. The infinitely wide beam is an approximation of the experimental hyperspectral irradiation, where wide-field illumination is used. A broad beam is assumed to be a beam where the size of the beam is substantially larger than the effective photon path length. Using the effective attenuation coefficient derived in the diffusion approximation,[22] the path length in dermis can be estimated to 1.0 and 1.3 mm in the simulated finger models at wavelengths 850 and 1080 nm, respectively. In epidermis, the path lengths are even shorter. The actual experimental beam size used in the available HSI setup is significantly wider than either of the estimated path lengths.

Photons entered into the VOI from the top xz VOI plane. They were partially reflected from the air–tissue boundary adding to specular reflection and partially transmitted into the finger model. All the exiting photons were registered as reflected (traveling backward) or transmitted (traveling forward). The reason for registering all photons was to improve statistics and consequentially decrease noise in the resulting spectra. Although the acceptance angle is much smaller in real hyperspectral cameras, similar results to the obtained ones are quantitatively expected for smaller acceptance angles.[39] The simulations presented here represent a generic case where the detection is inspired by, but not locked to a particular imaging system (Hyspex camera line, Norsk Elektro Optikk AS, Skedsmokoset, Norway). The hyspex cameras are push broom cameras, with a typical spectral resolution of 3.7-6 nm, and a spatial resolution dependent on the fore optics. For medical applications, the spatial resolution (pixel size) at the sample surface is typically 50 to 100 μm. The optics and configuration of these systems are designed to minimize spatial and spectral misregistration. The field of view of the camera aperture is 17 deg. Such cameras can be used for transmission or reflectance measurements depending on the chosen light source configuration. The signal-to-noise ratio (SNR) will depend on the applied irradiance from the light source; however, an acceptable SNR can be achieved within the exposure limits given by ICNIRP and ISO. Realistic experimental radiance values are comparable to the numbers achieved in this study.

Table 2 Tissue parameters of simulated tissue types in the simulated normal and arthritic human joints. N – normal joint, SF – joint with synovial fluid efflux, SM – joint with synovial membrane proliferation, SFM – joint with SF and SM. MVF – melanin volume fraction (%), BVF – blood volume fraction (%), O_2S – oxygen saturation (%), WVF – water volume fraction (%), FVF – fat volume fraction (%).

Tissue		N	SF	SM	SFM	References
Epidermis	MVF	0.7	0.7	0.7	0.7	μ_a,[22–24] μ_s,[25] g,[26] n[27]
Dermis	BVF	0.4	0.4	0.4	0.4	Bloodless dermis μ_a and μ_s,[25] g,[26] n[27] adding BVF of blood[23]
	O_2S	95	67	67	67	
	WVF	85	85	85	85	
Adipose	FVF	0.45	0.45	0.45	0.45	μ_a,[25,28,29] μ_s,[25] g[29], n[30]
Blood						[31]
Artery	O_2S	97	97	97	97	Blood
Vein	O_2S	67	67	67	67	Blood
Tendon	BVF	2	2	2	2	Dermis
	O_2S	95	48	48	48	
Synovial membrane	BVF	2.9	2.9	1.2	1.2	Mucous membrane[32] adding BVF of blood.
	O_2S	95	48	48	48	
Synovial fluid		Water	Synovial fluid	Synovial fluid	Synovial fluid	Water,[33,34] synovial fluid from arthritic knee joint[21]
Cartilage	WVF	75	90	90	90	μ_a and μ_s,[35] $g = 0.75$
Bone						μ_a and μ_s,[36] g,[37] n[38]

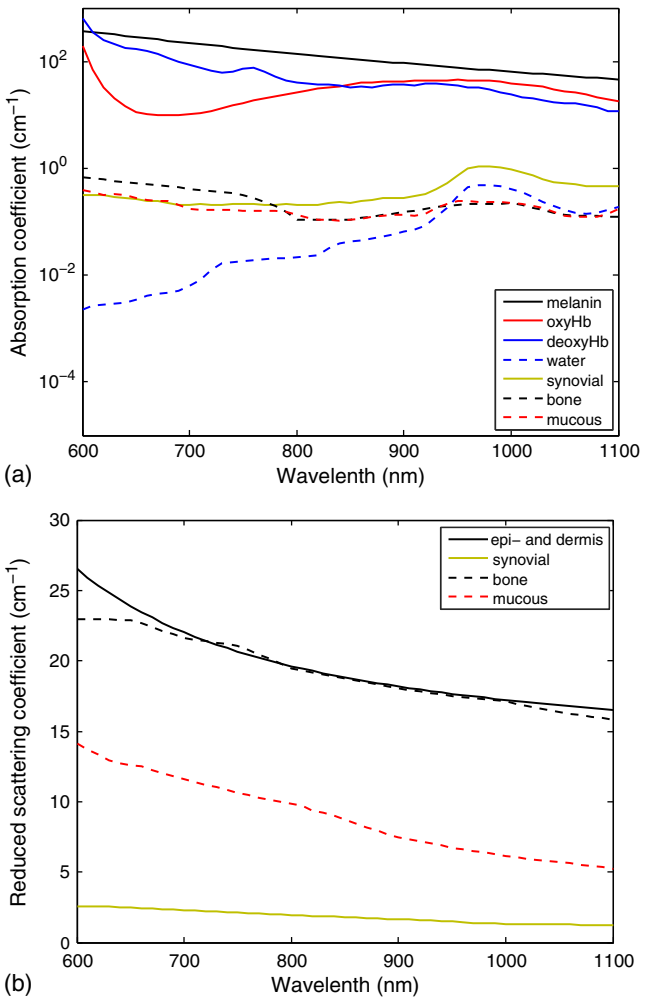

Fig. 3 (a) Absorption and (b) reduced scattering coefficients of the included chromophores.

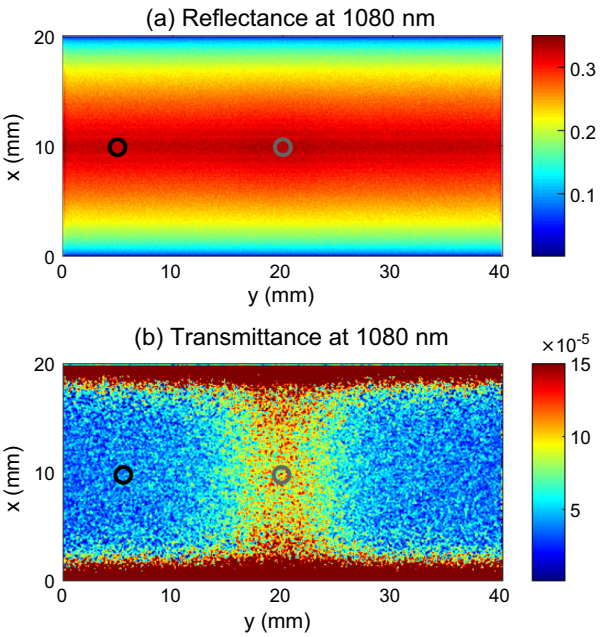

Fig. 4 (a) Reflectance and (b) transmittance image of the normal finger model at 1080 nm. Circles mark the areas from which the spectra presented in Fig. 4 were obtained (black–bone area, gray–cavity area).

The detection angle will depend on the entire optical system including the detector and fore optics, which will vary between the systems.

Diffuse reflectances and transmittances were determined for wavelengths between 600 and 1100 nm with a step size of 10 nm. The total number of simulated photons per wavelength and geometry was 50,000,000, but noise was still present in the results due to the statistical nature of MC. To improve SNR, the minimum noise fraction algorithm[40] was used for noise removal.

More information about the simulated experimental system can be found in Ref. 41. The final hyperspectral Iacobus system will be presented in a separate publication by the industrial partner.

4 Results and Discussion

To discover the spatial features of the normal finger model, the reflectance [Fig. 4(a)] and transmittance images [Fig. 4(b)] at 1080 nm are compared. This wavelength was chosen due to the large optical penetration depth at this wavelength. The reflectance image does not show any significant features along the finger, while the transmittance image features a distinct bright central region indicating the location of the joint cavity [Fig. 2(b)]. The bright region is a result of photons traversing the whole thickness of the joint. In the transversal direction, both images show a gradual change of brightness due to the surface curvature.

Simulated reflectance spectra [Fig. 5(a)] show characteristic spectral features of the tissue (see arrows). However, the difference between the spectra obtained above the joint cavity (light gray, Fig. 4 gray circle) and the region including the bone (black, Fig. 4 black circle) is negligible in the visible region due to high melanin absorption. The observed difference is relatively small in the near-infrared region (2% difference).

On the other hand, transmittance spectra show a significant amplitude difference between the joint cavity and bone regions. Specifically, the transmittance beneath the joint cavity is approximately two times larger than beneath the bone. Moreover, two optical windows can be observed: 800 to 900 nm and 1050 to 1100 nm. They result from minima in the absorption of major chromophores in these regions. The same minima as in the reflectance spectrum can be observed, but are more expressed due to longer photon path lengths.

The two transmission windows can be seen in the transmission spectrum along the finger axis as a function of the longitudinal coordinate y [Fig. 6(a)]. Here, two bright regions beneath the joint cavity are present for the 800 to 900 nm and 1050 to 1100 nm spectral regions. Bell-shaped longitudinal transmission profiles are presented in Fig. 6(b) for the central wavelengths of the transmission windows. The 850-nm profile is sharper than the 1080 profile, but both features are approximately the same full width at half maximum (FWHM) (8 mm). The same is true for increased melanin levels (Appendix). The most significant difference between the profiles obtained for different melanin levels is a general decrease of the transmittance while the shape is preserved.

Two distinct classes of photons contribute to the transmittance. The first class are photons that are scattered multiple times and travel within soft tissues encircling the bone. These

photons contribute to the transmittance both beneath the bone and beneath the cavity, i.e., the background transmittance. The second class are the photons traversing the whole thickness of the joint traveling through the relatively transparent cavity. These photons contribute only to transmittance near the cavity.

To discover the specific features of the affected joints, results from arthritic and normal joints were compared. In general, the transmission spectra of an arthritic joint gap [Fig. 7(a)] decrease compared to the normal joint, with the SF effusion model having the highest transmittance, followed by the mixed (SFM) model, and the synovial membrane thickening (SM) model having the lowest transmittance. The reduced transmittance of the arthritic joint is a result of both increased scattering and absorption in these joints. The fact that the SFM model transmittance is in-between the SF and SM transmittances is reasonable, since the properties of the former are a combination of the latter two. The spectra beneath the bone are equal for all simulated models.

A difference between the 800 to 900 nm and 1050 to 1100 nm transmission windows exists. For the first window, the SF model shows almost the same transmission as the normal joint, while the SM and SFM models have ~1.6× lower transmittance. For the second window, all models significantly show lower transmittance. Specifically, the SF model transmittance is decreased 1.4×. The observed difference is a consequence of a significantly lower scattering in the SF compared to the synovial membrane (~5×), and comparable absorption of both tissue types in the 800 to 900-nm spectral region. The scattering in both tissue types markedly decreases in the 1050 to 1100-nm spectral region, while absorption of the SF becomes ~2.7 × larger than the synovial membrane absorption. The observed difference could be used to distinguish between different forms of arthritis, namely SF, SM, and SFM forms.

The same trends as in the spectra are observed in the longitudinal profiles [Figs. 7(b) to 7(d)]. The SF model profile has broad bell-shaped peaks at 850 and 1080 nm with ~2× larger FWHM than the normal joint. Two smaller peaks are superimposed on the main peak. These features are artifacts due to the geometry and are located in the region where the affected tissue changes into normal finger. The simulated transition was discrete, while in a real finger it is more diffuse.

For 1080 nm, the SM model profile is similar to the SF profile featuring a bell-shaped peak of small amplitude. However, the profile features decreased transmission in the joint region at 850 nm. The transmission in the joint region is on average 12% lower than in the bone region. The same effect is observed in the

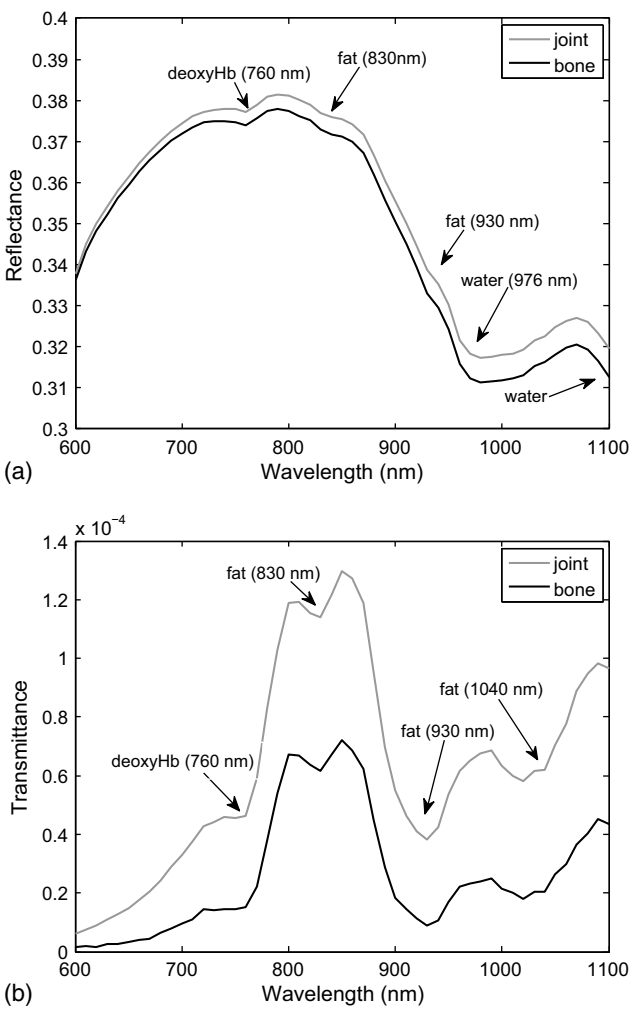

Fig. 5 (a) Reflectance and (b) transmittance spectra in the region of joint (light gray) and bone (black).

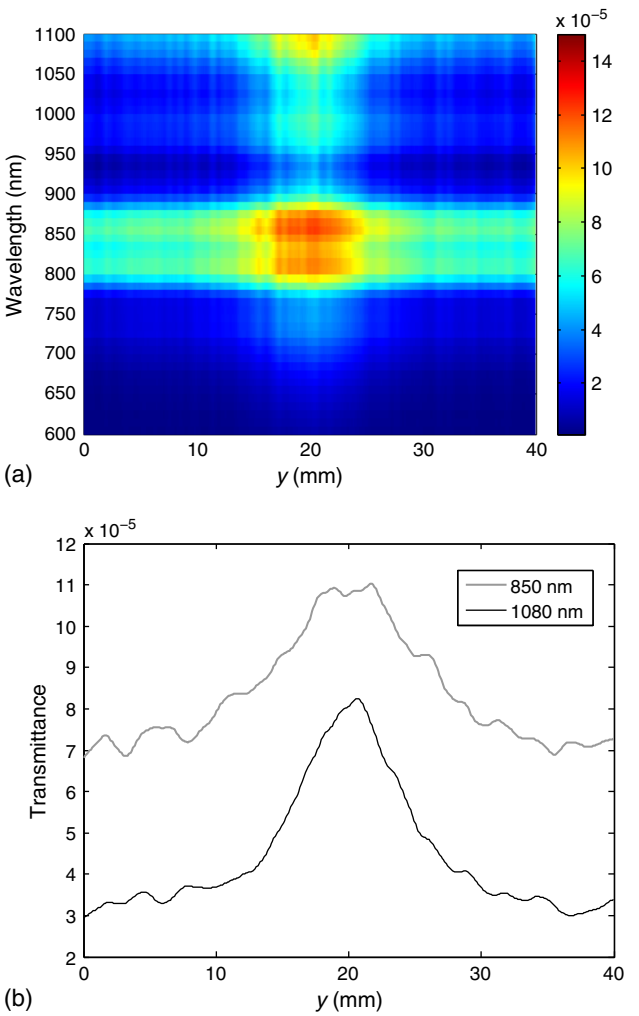

Fig. 6 (a) Transmittance spectrum along the finger axis and (b) corresponding axial transmittances at 850 and 1080 nm for the normal joint.

SFM model profiles for both regions. In addition, a local bell-shaped peak is present due to the increased SF volume. The observed decrease of the transmission in the SM and SFM models, especially expressed at 850 nm, is due to the synovial membrane thickening and consequential increased scattering. The differences in the spatial transmittance distribution can also be exploited to discriminate between different forms of arthritis.

The reflectance results obtained for the affected joints are similar to the normal joint results.[21] A small difference (~2%) exists between the affected and the normal joints, which could be difficult to observe in experimental data due to measurement noise. Counterintuitively, the reflectance results displayed no significant spatial or spectral features that could help in discriminating between the arthritic and the normal joints.

The finger models used in this study do not completely resemble the true geometry and physiology of a human joint. Therefore, the presented results can differ from experimental results to some extent. In our models, vasculature in an inflamed synovial membrane was simulated as a total change in blood volume fraction. However, in the real membrane, discrete vessels are present and these vessels might actually be detectable in the reflectance and transmission images. Oxygenation and blood volume fraction in dermis are uncertain as no values for such properties in arthritic fingers exist in the available literature. Moreover, the changes in skin anatomy of an inflamed joint might affect the optical parameters. For example, skin thickness can be reduced and skin ridges flattened due to skin stretching due to swelling of the joint. In addition, it should be pointed out that the morphological and physiological changes included in the studied arthritis models might not be so well pronounced in actual early stage arthritis. These models were constructed based on the average values reported for well-developed rheumatic arthritis samples. To be able to construct a model for early detection of arthritis, it is important to have precise knowledge about how the various features present in advanced cases first. Based on that, it is possible to construct algorithms detecting the various features and validate them against early stage cases. However, the benefit of simulating pronounced changes over simulating very small changes is that the arthritis related features are more expressed in the simulated spectra. Thus, it is easier to identify these features and optimal imaging parameters (spectral ranges, reflectance, or transmittance). We believe that similar, albeit possibly less expressed, features would be identified in early arthritis hyperspectral images. This will be experimentally validated in an upcoming study.

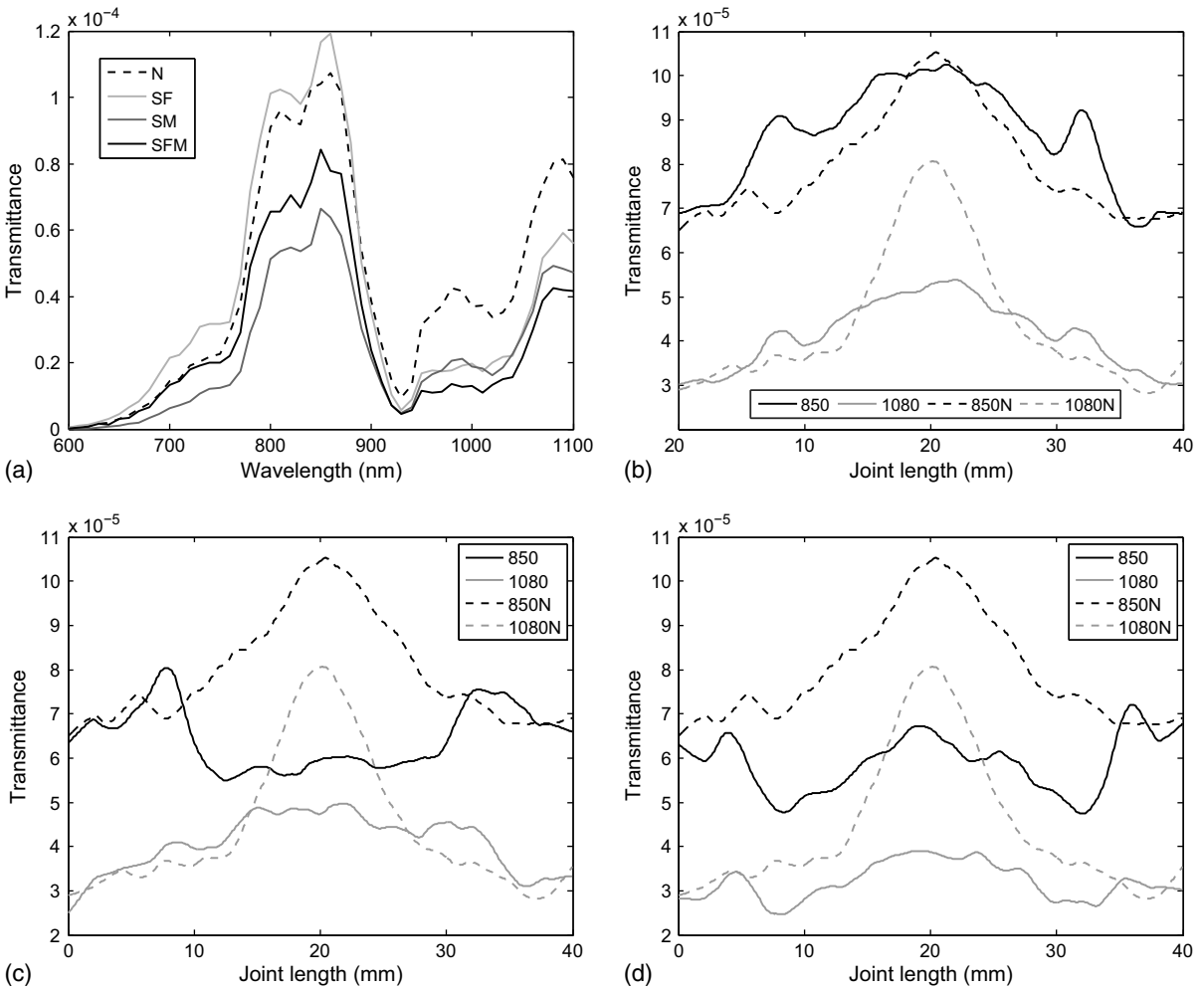

Fig. 7 (a) Transmission spectra below the joint gaps for all simulated models. (b) Longitudinal transmission profiles at 850 nm (black) and 1080 nm (gray) for the SF, (c) SM, and (d) SFM models. The transmission profiles of the normal joint are added for comparison (dashed, letter N in legend).

Transmittance is found to be a very sensitive tool for detecting changes in joints, since both absorption and scattering modulate the spectral and spatial characteristics of transmitted light. One other group has explored the applicability of transmittance for detecting joint arthritis.[42,6] They studied transillumination through a joint using a laser at 635 nm and observed a substantial decrease in transmittance through an arthritic joint compared to a healthy joint. In addition, they demonstrated that the transmitted light has a bell-shaped spatial distribution, which agrees well with our results [Figs. 7(b) to 7(d)].

In this study, transmission and reflectance spectra were simulated to identify spectral features that can be used in developing an optical diagnostic system for detection of arthritis. The purpose of this study was to study the feasibility of the technique and to identify optimal imaging parameters. An actual system would have specific optics the limiting acceptance angle to angles significantly smaller than the 180 deg simulated here, detectors with specific sensitivities and SNRs, and light sources with specific spectra and powers. All this could result in hyperspectral images which would quantitatively differ from the images presented here, but the same qualitative spectral features are expected to be present. A future experimental study using an actual hyperspectral system will be performed to verify the simulation results and experimentally confirm the feasibility of the technique.

An important result of this study are the two optical windows, 800 to 900 nm and 1050 to 1100 nm, which might be important for arthritis diagnosis. Changes in transmission can be attributed to changes in scattering due to changes in the SF or synovial membrane, edema, or changes in the vascularization of the joint. In addition to transmission changes in these wavelength windows, it is expected that blood content and localization will be important parameters for a final diagnostic algorithm.

5 Conclusions

The main objective of this study was to explore the feasibility of HSI in arthritis diagnostics through simulation of transmission and reflectance spectra in the 600 to 1100-nm wavelength range, and to identify optimal imaging parameters. It was demonstrated that transmittance images of human joints could be used as one parameter for discrimination between arthritic and unaffected joints. By analyzing simulation results, two transmission spectral windows were identified where enhanced transmission is obtained. Specifically, the transmission windows were 800 to 900 nm and 1050 to 1100 nm. Reflectance spectra were not sensitive to changes in the affected joint.

The numerical model served as an important tool for the understanding and development of HSI as an arthritis diagnostic modality. Promising specific spectral and spatial features for the diagnostics and follow-up monitoring of small joint arthritis were discovered. An experimental study is planned to verify the findings of the simulations, and to identify further parameters needed for early hyperspectral diagnosis of arthritis.

Appendix: Darker Skin Types

In the simulations, the melanin volume fraction (MVF) in the epidermal layer was 0.7% for all simulated joints, which corresponds to light Caucasian skin. The light Caucasian skin type was chosen for the simulations in order to obtain good agreement with the experimental measurements (not included here), since the majority of the subjects included in these measurements have this type of skin. To evaluate the effect of melanin on transmitted light, the HSI of the normal finger model was simulated with MVFs of 2.5% and 5.0%, a Mediterranean skin and dark skin, respectively. Results for the wavelengths 850 and 1080 nm are presented in Fig. 8. Evidently, increased melanin reduces amplitudes—12% and 33% reduction compared to the light Caucasian skin at 850 nm [Fig. 8(a)], and 6% and 18% reduction at 1080 nm [Fig. 8(b)]. However, the bell-shaped profile is still present. The difference in transmittances due to a change in melanin levels could be compensated by using the reflectance data. It is possible to determine MVF by analyzing the reflectance.[29]

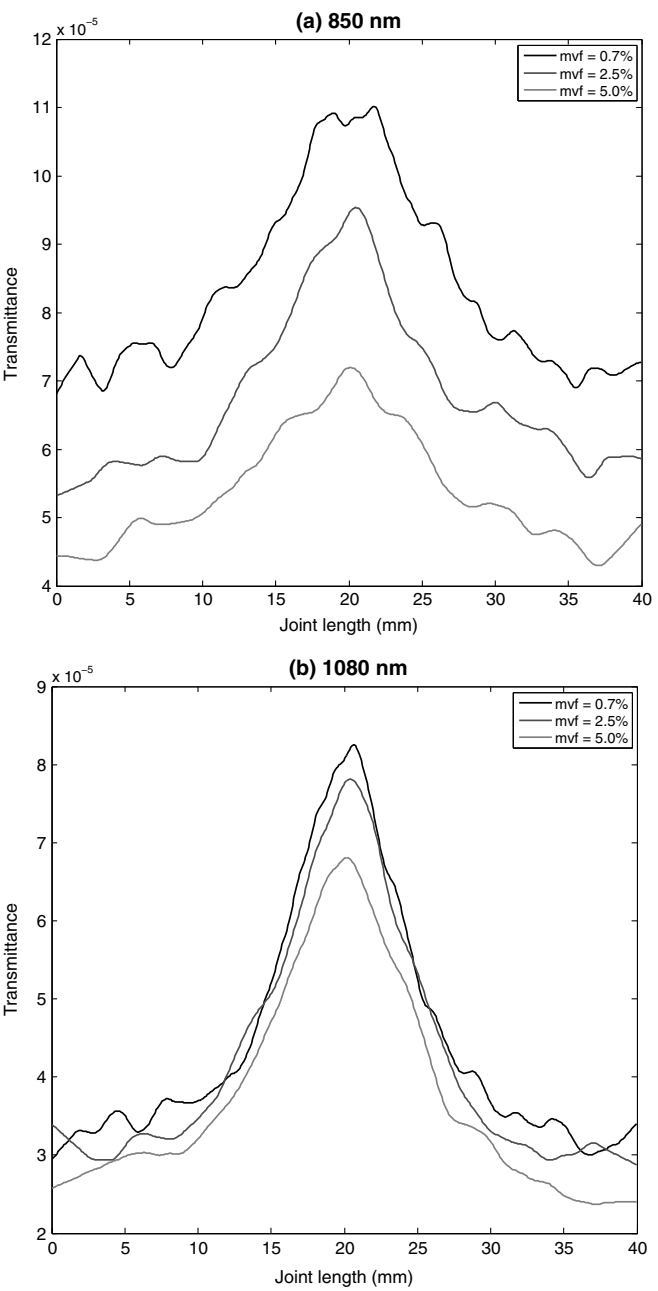

Fig. 8 Longitudinal transmission profiles for the normal joint model at (a) 850 nm and (b) 1080 nm. Simulated melanin volume fractions were 0.7%, 2.5%, and 5%.

Acknowledgments

This work was supported by the European Commission under the 7th Framework Programme for the Collaborative Project under Grant No. 305760 (IACOBUS). The authors would like to thank Dr. Berit Grandaunet at Norwegian University of Science and Technology for providing samples of synovial fluid.

References

1. A. C. Rat and M. C. Boissier, "Rheumatoid arthritis: direct and indirect costs," *Jt. Bone Spine* **71**(9), 518–524 (2004).
2. J. A. B. van Nies et al., "What is the evidence for the presence of a therapeutic window of opportunity in rheumatoid arthritis? A systematic literature review," *Ann. Rheum. Dis.* **73**(5), 861–870 (2014).
3. K. Raza et al., "Treating very early rheumatoid arthritis," *Best Pract. Res. Clin. Rheumatol.* **20**(5), 849–863 (2006).
4. K. Raza et al., "Early rheumatoid arthritis is characterized by a distinct and transient synovial fluid cytokine profile of T cell and stromal cell origin," *Arthritis Res. Ther.* **7**(4), R784–R795 (2005).
5. D. Chamberland, Y. B. Jiang, and X. D. Wang, "Optical imaging: new tools for arthritis," *Integr. Biol.* **2**(10), 496–509 (2010).
6. J. Beuthan et al., "Light scattering study of rheumatoid arthritis," *Quantum Electron.* **32**(11), 945–952 (2002).
7. L. D. Montejo et al., "Computer-aided diagnosis of rheumatoid arthritis with optical tomography, Part 1: feature extraction," *J. Biomed. Opt.* **18**(7), 076001 (2013).
8. L. D. Montejo et al., "Computer-aided diagnosis of rheumatoid arthritis with optical tomography, Part 2: image classification," *J. Biomed. Opt.* **18**(7), 076002 (2013).
9. B. S. Sorg et al., "Hyperspectral imaging of hemoglobin saturation in tumor microvasculature and tumor hypoxia development," *J. Biomed. Opt.* **10**(4), 044004 (2005).
10. L. L. Randeberg, E. L. Larsen, and L. O. Svaasand, "Characterization of vascular structures and skin bruises using hyperspectral imaging, image analysis and diffusion theory," *J. Biophotonics* **3**(1–2), 53–65 (2010).
11. M. Klarlund, M. Ostergaard, and I. Lorenzen, "Finger joint synovitis in rheumatoid arthritis: quantitative assessment by magnetic resonance imaging," *Rheumatology* **38**(1), 66–72 (1999).
12. C. R. Stevens et al., "A comparative-study by morphometry of the microvasculature in normal and rheumatoid synovium," *Arthritis Rheum.* **34**(12), 1508–1513 (1991).
13. A. Aberman et al., "An equation for oxygen hemoglobin dissociation curve," *J. Appl. Physiol.* **35**(4), 570–571 (1973).
14. J. M. Mountz, A. Alavi, and J. D. Mountz, "Emerging optical and nuclear medicine imaging methods in rheumatoid arthritis," *Nat. Rev. Rheumatol.* **8**(12), 719–728 (2012).
15. J. M. G. Canvin et al., "Infrared spectroscopy: shedding light on synovitis in patients with rheumatoid arthritis," *Rheumatology* **42**(1), 76–82 (2003).
16. R. A. Shaw et al., "Arthritis diagnosis based upon the near infrared spectrum of synovial fluid," *Rheumatol. Int.* **15**(4), 159–165 (1995).
17. D. Podolsky et al., "Comparison of third toe joint cartilage thickness to that of the finger proximal interphalangeal (PIP) joint to determine suitability for transplantation in PIP joint reconstruction," *J. Hand Surg. Am.* **36**(12), 1950–1958 (2011).
18. D. Howell, "Etiopathogenesis of osteoarthritis," in *Arthritis and Allied Conditions* D. J. McCarty, Ed., Lea and Febiger, Philadelphia (1989).
19. T. B. Möller and E. Reif, Eds., *Pocket Atlas of Sectional Anatomy: Computed Tomography and Magnetic Resonance Imaging*, 3rd ed., Thieme, Stuttgart, New York (2007).
20. S. H. Pheasant and C. M. Haslegrave, *Bodyspace: Anthropometry, Ergonomics and the Design of Work*, CRC Press, Boca Raton, Florida (2005).
21. M. Milanic, L. A. Paluchowski, and L. L. Randeberg, "Simulation of light transport in arthritic- and non-arthritic human fingers," *Proc. SPIE* **8936**, 893602 (2014).
22. L. O. Svaasand et al., "Tissue parameters determining the visual appearance of normal skin and port-wine stains," *Laser Med. Sci.* **10**(1), 55–65 (1995).
23. M. Milanic and B. Majaron, "Three-dimensional Monte Carlo model of pulsed-laser treatment of cutaneous vascular lesions," *J. Biomed. Opt.* **16**(12), 128002 (2011).
24. S. L. Jacques, "Optical properties of biological tissues: a review," *Phys. Med. Biol.* **58**(11), R37–R61 (2013).
25. E. Salomatina et al., "Optical properties of normal and cancerous human skin in the visible and near-infrared spectral range," *J. Biomed. Opt.* **11**(9), 064026 (2006).
26. S. V. Patwardhan, A. P. Dhawan, and P. A. Relue, "Monte Carlo simulation of light-tissue interaction: three-dimensional simulation for trans-illumination-based Imaging of skin lesions," *IEEE Trans. Biomed. Eng.* **52**(7), 1227–1236 (2005).
27. H. F. Ding et al., "Refractive indices of human skin tissues at eight wavelengths and estimated dispersion relations between 300 and 1600 nm," *Phys. Med. Biol.* **51**(9), 1479–1489 (2006).
28. R. L. P. van Veen et al., "Determination of VIS–NIR absorption coefficients of mammalian fat, with time- and spatially resolved diffuse reflectance and transmission spectroscopy," presented at *OSA Ann. Biomed. Top. Mtg.*, Miami Beach, Florida, Paper SF4, Optical Society of America (2004).
29. A. Bjorgan, M. Milanic, and L. L. Randeberg, "Estimation of skin optical parameters for real-time hyperspectral imaging applications," *J. Biomed. Opt.* **19**(9), 066003 (2014).
30. G. J. Müller and A. Roggan, *Laser-Induced Interstitial Thermotherapy*, SPIE Press, Bellingham, Washington (1995).
31. M. Friebel et al., "Influence of oxygen saturation on the optical scattering properties of human red blood cells in the spectral range 250 to 2000 nm," *J. Biomed. Opt.* **14**(3), 034001 (2009).
32. A. N. Bashkatov et al., "Optical properties of mucous membrane in the spectral range 350-2000 nm," *Opt. Spectrosc.* **97**(9), 978–983 (2004).
33. R. C. Smith and K. S. Baker, "Optical properties of the clearest natural-waters (200–800 Nm)," *Appl. Opt.* **20**(2), 177–184 (1981).
34. L. H. Kou, D. Labrie, and P. Chylek, "Refractive indexes of water and ice in the 0.65-Mu-M to 2.5-Mu-M spectral range," *Appl. Opt.* **32**(19), 3531–3540 (1993).
35. D. W. Ebert et al., "Articular cartilage optical properties in the spectral range 300–850 nm," *J. Biomed. Opt.* **3**(3), 326–333 (1998).
36. A. N. Bashkatov et al., "Optical properties of human cranial bone in the spectral range from 800 to 2000 nm," *Proc. SPIE* **6163**, 616310 (2006).
37. N. Ugryumova, S. J. Matcher, and D. P. Attenburrow, "Measurement of bone mineral density via light scattering," *Phys. Med. Biol.* **49**(3), 469–483 (2004).
38. A. Ascenzi and C. Fabry, "Technique for dissection and measurement of refractive index of osteones," *J. Biophys. Biochem. Cytol.* **6**(1), 139 (1959).
39. L. L. W. Randeberg et al., "Performance of diffusion theory versus Monte Carlo methods," *Proc. SPIE* **5862**, 58620O (2005).
40. A. A. Green et al., "A transformation for ordering multispectral data in terms of image quality with implications for noise removal," *IEEE Trans. Geosci. Remote Sens.* **26**(1), 65–74 (1988).
41. L. A. Paluchowski et al., "Identification of inflammation sites in arthritic joints using hyperspectral imaging," *Proc. SPIE* **8947**, 89470H (2014).
42. O. Minet et al., "Optical monitoring of rheumatoid arthritis: Monte Carlo generated reconstruction kernels," *Proc. SPIE* **6791**, 67910G (2008).

Matija Milanic received his PhD in physics from the University of Ljubljana in 2008. Since 2003, he has worked as a research assistant at Jožef Stefan Institute, Slovenia. His research interests include interaction of light with biological tissues, from photothermal radiometry, spectroscopy, and imaging to numerical simulations. Currently, he completed postdoctoral training at Norwegian University of Science and Technology in Trondheim.

Biographies for the other authors are not available.